Rev. Roum. Sci. Techn.– Électrotechn. et Énerg.
Vol. **68**, *1*, pp. 46–51, Bucarest, 2023

CONTROL OF DOUBLY-FED INDUCTION GENERATOR USING ARTIFICIAL NEURAL NETWORK CONTROLLER

IBRAHIM YAICHI[1, 2], ABDELHAFID SEMMAH[2], PATRICE WIRA[3]

Keywords: Variable speed wind turbine; Doubly fed induction generator; Field oriented control; Conventional direct power control; Total harmonic distortion; Maximum power point tracking; Artificial neural network.

In this paper, we propose a direct power control (DPC) based on an artificial neural network (ANN-DPC) for the doubly-fed induction generator (DFIG), which is applied to the wind turbine system. The main objective of this intelligent technique is to replace the switching table and the hysteresis comparators with a neural control to reduce the ripple to the level of current and power. Field-oriented control (FOC) is traditionally achieved using a conventional proportional-integral controller (PI). The power ripples are reduced, and a reasonable total harmonic distortion rate is ensured by using an ANN-DPC.

1. INTRODUCTION

Given the extent of industrialization in recent decades, the demand for electric power has become very important, which has resulted in a decrease in the global stock of hydrocarbons. Faced with this and the challenge of global warming of the earth caused by greenhouse gas emissions linked to the excessive consumption of energy from fossil materials (oil, coal, natural gas, etc.), it is out necessary to use new sources of energy (renewable) that will be without consequences for man and the environment [1].

After centuries of evolution and further research in recent decades, several countries have now turned their attention to wind energy [2].

The new interest in wind energy since the mid-1970s is the result of two concerns: On the one hand, the protection of the environment and the resulting fossil fuel economy. On the other hand, the evolution of technologies makes converting this energy more and more profitable. Therefore, its use becomes economically competitive compared to traditional sources of the same power [3].

The latest generation of wind turbines operates at variable speeds. This operation makes it possible to increase energy efficiency, decrease mechanical efforts, and improve the quality of electrical energy produced compared to fixed-speed wind turbines. It is the development of electronic variators, which makes it possible to control the speed of rotation of the wind turbines at every moment. The wind is a random size of a very fluctuating nature. The variations in the resulting power of wind fluctuations are the main disturbance of the wind energy conversion chain [3].

The first application developed was the control of an electrical machine, and the control structure was known as Direct Torque Control (DTC). In this case, the machine's stator flux and electromagnetic torque are controlled without any modulation block. Then, a similar technique, but applied to the power, called Direct Power Control (DPC) was proposed by H. Nian in [4] and developed later by M. Malinowski in [5] for a control application of the rectifiers in replacement of the traditional command based on the regulation of current loops. In this new control technique, the controlled variables are the instant active and reactive powers.

Artificial Neural Networks (ANN) are well known for their ability to learn and approximate any continuous function. They were applied to the identification of the parameters and the estimation in the state space of the control systems of the reciprocating engines [2, 6].

The results of the control simulations (FOC), (C-DPC), and (ANN-DPC) proposed are compared for different step variations of the active and reactive power. The reference of the reactive power can be kept at zero to ensure the operation of the unit power factor.

2. WIND TURBINE MODEL

The wind speed or wind power is defined as follows [7]:

$$P_v = \frac{1}{2}\rho S V^3, \tag{1}$$

where P_v is the total power theoretically available; ρ is the density of the air (1.22 kg/m³ at atmospheric pressure at 15 ºC); S is the circular surface swept by the turbine, and the length of the blade determines the radius of the circle, and v is the wind speed.

The conversion device (the wind turbine) extracts aerodynamic power P_{aer} less than the available power P_v.

$$P_{aer} = C_p.P_v = C_p(\beta,\lambda)\frac{1}{2}\rho S v^3. \tag{2}$$

The power factor C_p represents the aerodynamic efficiency of the wind turbine (P_{aer} /P_v). It depends on the turbine's characteristics [8, 9].

This coefficient varies with the angle of orientation of the blades (β) and the speed ratio (λ).

The speed ratio is defined as the ratio between the linear speed of the blades and the wind speed:

$$\lambda = R\frac{\Omega_{turbine}}{v}, \tag{3}$$

where $\Omega_{turbine}$ is the speed of the turbine and R is the radius of the wind turbine.

Knowing the speed of the turbine, the aerodynamic torque is directly determined by:

$$C_{aer} = \frac{P_{aer}}{\Omega_{turbine}} = C_p\frac{1}{2}\rho S v^3\frac{1}{\Omega_{turbine}}. \tag{4}$$

The power coefficient expression of a 1.5 MW wind

[1] Laboratoire de Developpement Durable et d'Informatique (LDDI), Ahmed Draya University, 01000 Adrar, Algeria, E-mail: ibrahimyaichi@gmail.com
[2] Department of Electrical Engineering, Faculty of Electrical Engineering, Djillali Liabes University, 022000 Sidi Bel Abbes, Algeria. E-mail: hafid.semmah@yahoo.fr
[3,4] Institut de Recherche en Informatique, Mathématiques, Automatique et Signal (IRIMAS), Université de Haute Alsace, 68093 Mulhouse, France. E-mail : patrice.wira@uha.fr

turbine is approximated by equation [10, 11]:

$$C_p(\beta,\lambda)=\left(0.5\text{-}0.0167(\beta\text{-}2)\right)\sin\left[\frac{\pi(\lambda+0.1)}{18.5\text{-}0.3(\beta+2)}\right]- \\ -0.00184(\lambda\text{-}3)(\beta\text{-}2). \quad (5)$$

The speed multiplier is the link between the turbine and the generator. It aims to adapt the speed of the turbine $\Omega_{turbine}$, relatively slower than that required by the generator Ω_g [12, 13].

Figure 1 shows the wind profile used to study a variable-speed wind system.

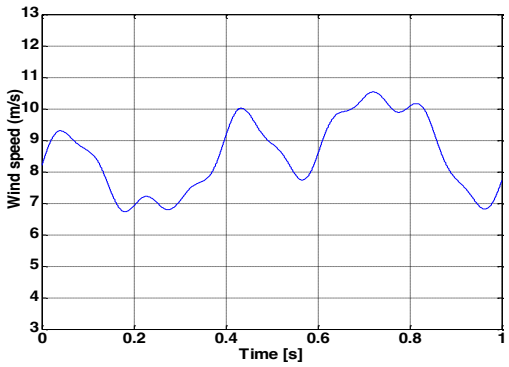

Fig. 1 – Profile of the wind speed.

The proportional-integral regulator (PI) used to control the speed of rotation and to attenuate the effect of the torque of the DFIG C_g considered as a disturbance. The block diagram of the MPPT control is illustrated in Fig. 2.

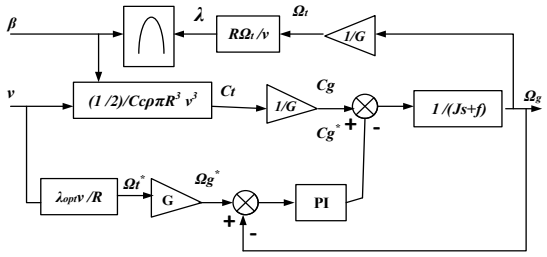

Fig. 2 – MPPT control of DFIG.

3. MODELING OF THE DFIG

In the synchronous d-q reference frame rotating at ω_s speed, the model of the DFIG is given by the following equations [14]:

Rotor and stator components:

$$\begin{cases} V_{ds} = R_s I_{ds} + \frac{d\Psi_{ds}}{dt} - \omega_s \Psi_{qs} \\ V_{qs} = R_s I_{qs} + \frac{d\Psi_{qs}}{dt} - \omega_s \Psi_{ds} \\ V_{dr} = R_r I_{dr} + \frac{d\Psi_{dr}}{dt} - (\omega_s - \omega_r)\Psi_{qr} \\ V_{qr} = R_r I_{qr} + \frac{d\Psi_{qr}}{dt} - (\omega_s - \omega_r)\Psi_{dr} \end{cases}, \quad (6)$$

Rotor and stator flux components:

$$\begin{cases} \Psi_{ds} = L_s I_{ds} + M\, I_{dr} \\ \Psi_{qs} = L_s I_{qs} + M\, I_{qr} \\ \Psi_{dr} = L_r I_{dr} + M\, I_{ds} \\ \Psi_{qr} = L_r I_{qr} + M\, I_{qs} \end{cases}. \quad (7)$$

The electromagnetic torque is also expressed as a function of currents and flux by:

$$C_{em} = \frac{3}{2}\frac{M}{L_s} p(\Psi_{qs} I_{dr} - \Psi_{ds} I_{qr}). \quad (8)$$

Mechanical equation:

$$J\frac{d\Omega}{dt} = C_{em} - C_r - f\Omega, \quad (9)$$

In the two-phase reference, the active and reactive stator powers of a DFIG are written according to:

$$\begin{cases} P_s = \frac{3}{2}(V_{ds} I_{ds} + V_{qs} I_{qs}), \\ Q_s = \frac{3}{2}(V_{qs} I_{ds} - V_{ds} I_{qs}). \end{cases} \quad (10)$$

4. FIELD ORIENTED CONTROL STRATEGY

Given the vector control of the DFIG, it is better to choose the d-q mark linked to the stator rotating field relative to the frequency of 50 Hz (mains frequency). Therefore, the Park reference will be synchronized with the stator flux (Fig. 2) [15, 16].

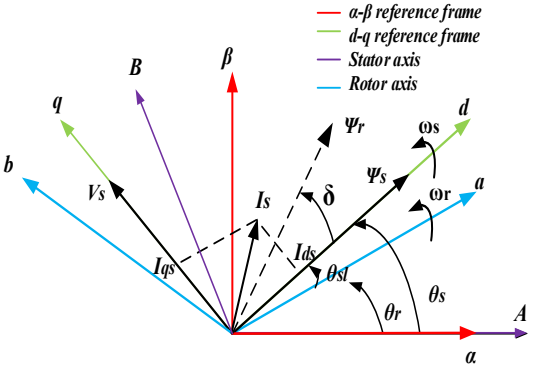

Fig. 3 – Stator field-oriented control technique.

Often in the case of a medium and high-power DFIG, the stator resistance R_s is neglected during the synthesis of its model under the assumption of stator flux orientation [17, 18].

By adopting the hypothesis of a stator resistance Rs that is negligible, and that the stator flux is constant (this condition is ensured in the case of a stable network connected to the stator of the DFIG), and oriented along the axis d, one deduced [19, 20]:

$$\begin{cases} \Psi_{qs} = 0 \\ \Psi_{ds} = \Psi_s \end{cases}, \quad (11)$$

$$\begin{cases} V_{ds} = 0 \\ V_{qs} = V_s = \omega_s V_s \end{cases}, \quad (12)$$

$$\begin{cases} \Psi_s = L_s I_{ds} + M\, I_{dr} \\ 0 = L_s I_{qs} + M\, I_{qr} \end{cases}. \quad (13)$$

From eq. (13), we can then write the equations linking the stator currents to the rotor currents:

$$\begin{cases} I_{sd} = \frac{\Psi_s}{L_s} - \frac{M}{L_s} I_{dr} \\ I_{sq} = -\frac{M}{L_s} I_{qr} \end{cases}, \quad (14)$$

$$\begin{cases} P_s = \frac{3}{2} V_s I_{qs} \\ Q_s = \frac{3}{2} V_s I_{ds} \end{cases}. \quad (15)$$

Replacing the stator currents by their expressions given in (15), the equations below are expressed:

$$\begin{cases} P_s = -\frac{3}{2}\frac{M}{L_s} V_s I_{qr} \\ Q_s = \frac{3}{2} V_s \left(\frac{V_s}{L_s \omega_s} - \frac{M}{L_s} I_{dr}\right) \end{cases}. \quad (16)$$

The electromagnetic torque is as follows.

$$C_{em} = -\frac{3}{2} p \frac{M}{L_s} \Psi_s I_{qr} \quad (17)$$

To control the DFIG, expressions show the relationship between the currents and the rotor voltages applied to it.

$$V_{dr} = R_r I_{dr} + (L_r - \frac{M^2}{L_s})\frac{dI_{dr}}{dt} - g(L_r - \frac{M^2}{L_s})\omega_s I_{qr} \quad (18)$$

$$V_{qr} = R_r I_{qr} + \left(L_r - \frac{M^2}{L_s}\right)\frac{dI_{qr}}{dt} + \\ + g\left(L_r - \frac{M^2}{L_s}\right)\omega_s I_{dr} + g\frac{MV_s}{L_s}. \quad (19)$$

5. DIRECT POWER CONTROL OF THE DFIG

The study of literature is sometimes surprising. Generally, the systems evolve on bases at the origin very simply and become complex with time. The transition from vector control to direct torque and flow control (DTC) is marked by a significant simplification of the control algorithm. Only one could wonder why the development of the direct control of the active and reactive powers (DPC) did not occur before the command DTC [21, 22].

The active and reactive powers are given by the following relations [23, 24]:

$$\begin{cases} P_s = -\frac{3}{2}\frac{M}{\sigma L_s L_r} V_s \Psi_{r\beta} \\ Q_s = \frac{3}{2}\left(\frac{V_s}{\sigma L_s}\Psi_s - \frac{V_s M}{\sigma L_s L_r}\Psi_{r\alpha}\right) \end{cases} \quad (20)$$

where:

$$\begin{cases} \Psi_{r\alpha} = \sigma L_r i_{r\alpha} + \frac{M}{L_s}\Psi_s \\ \Psi_{r\beta} = \sigma L_r i_{r\beta} \\ |\overrightarrow{\Psi_s}| = \frac{|\overrightarrow{V_s}|}{\omega_s} \\ \sigma = 1 - \frac{M^2}{L_s L_r} \end{cases}, \quad (21)$$

If by introducing the angle δ between Ψ_s and Ψ_r, P_s and Q_s become [25]:

$$\begin{cases} P_s = -\frac{3}{2}\frac{M}{\sigma L_s L_r}\omega_s |\Psi_s||\Psi_r| \sin\delta \\ Q_s = \frac{3}{2}\frac{\omega_s}{\sigma L_s}|\Psi_s|(\frac{M}{L_r}|\Psi_r|\cos\delta - |\Psi_s|) \end{cases} \quad (22)$$

The following relation gives the variation of two active and reactive powers:

$$\begin{cases} \frac{dP_s}{dt} = -\frac{3}{2}\frac{M}{\sigma L_s L_r}\omega_s |\Psi_s| \frac{d(|\Psi_r|\sin\delta)}{dt} \\ \frac{dQ_s}{dt} = \frac{3}{2}\frac{M\omega_s}{\sigma L_s L_r}|\Psi_s| \frac{d(|\Psi_r|\cos\delta)}{dt} \end{cases} \quad (23)$$

The stator's active and reactive powers can then be varied by changing the angle between the rotor and stator vectors:

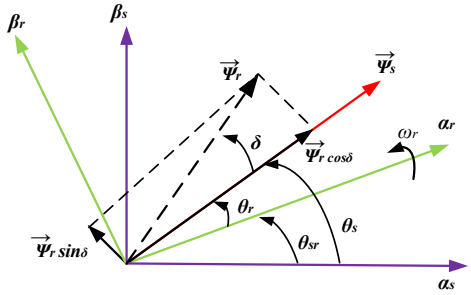

Fig. 4 – Rotor flux vector (α-β).

To determine the angles required for the Park transformations for the rotor (θr) and stator magnitudes (θs), we used a phase-locked loop (PLL). This PLL estimates the amplitude of the network voltage with precision and frequency.

6. NEURONAL DIRECT POWER CONTROL (ANN-DPC) STRATEGY

An ANN is not programmed; it is driven through a learning mechanism. Tasks particularly suited to neural network processing are association, classification, discrimination, prediction or estimation, and control of complex processes [26].

A neuron is a particular cell, as shown in Fig. 5. It has extensions by which it can distribute signals (axons) or receive them (dendrites) [26].

The multi-layered perceptron (MLP) is widely used in identification and control. With a hidden layer, it constitutes a "universal approximator".

One of the most common algorithms is back-propagation; this algorithm changes the weights of a network whose architecture is fixed by the operator whenever an example $y_i = f(x_i)$ is presented. This change is done in such a way as to minimize the error between the desired output and the response of the network to an input x_i. This is achieved thanks to the gradient descent method [27].

The input signal propagates in the network at each iteration in the input-output direction. An output is thus obtained, the error between this output and the desired output is calculated, and then by back-propagation, errors intermediates corresponding to the hidden layer are thus calculated and allow the adjustment of the weights $w_{ij}(t)$ of the hidden layer [27].

The algorithm for the backpropagation of the gradient comprises 2 phases:

- Propagation: The network is presented with an example input at each stage. This input is propagated to the output layer.
- Correction: Surely, the network will not provide exactly what was expected. Therefore, an error (usually the mean squared sum of errors for all output neurons) that is backpropagated in the network is calculated. This process is interrupted when the overall error is deemed sufficient [28].

To realize the learning of a MLP, one uses the generalized delta learning rule for each neuron i

$$w_{ij}(t+1) = w_{ij}(t) + \alpha(t)\delta_i(t)x_i \quad (24)$$

where $\delta_i(t)$ is the error made by the neuron i.

An example with a two-input network, three neurons in a hidden layer, and two neurons in the output layer is shown in Fig. 5.

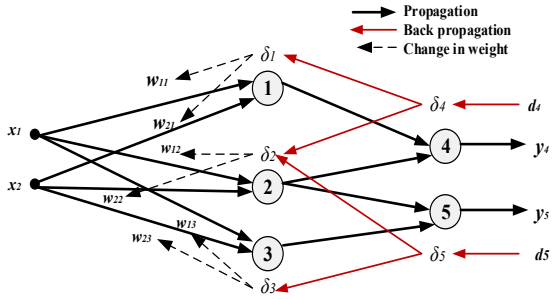

Fig. 5 – Back propagation algorithm for a MLP

To be able to modify the synaptic weights connecting the input layer to the hidden layer (w_{11}; w_{12}; w_{13} and w_{21}; w_{22}; w_{23}), it is necessary to know the desired outputs d_1, d_2 and d_3 which make it possible to apply the rule of the delta widespread [26, 28].

The idea is then to propagate the errors δ_4 and δ_5

towards the neurons 1, 2, and 3 through the weights w_{14}, w_{24}, w_{25}, and w_{35}, hence the name of backpropagation of the error gradient [28].

The neural network diagram of the proposed method is shown in Fig. 6.

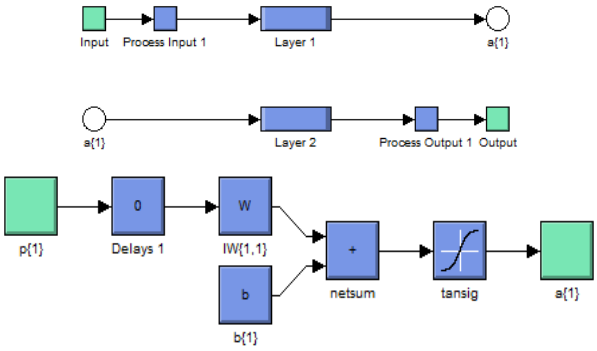

Fig. 6 – The neural network diagram of the proposed method

ANN-DPC structure of the DFIG is shown in Fig. 7.

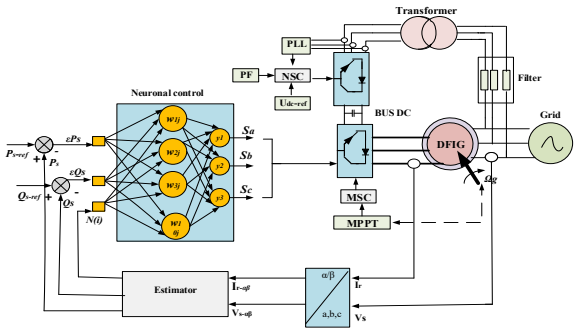

Fig. 7 – Schematic diagram of the ANN-DPC applied to DFIG

The hysteresis comparators and switching table C-DPC are replaced by a neural controller, whose inputs are the error of the active power εP_s, the reactive power εQ_s, and the position (zone) of the rotor flow Z (i). The outputs are the pulses S_a, S_b, S_c allowing the control of the inverter switches.

Table 1 presents the main parameters of the DFIG simulation model. The wind turbine parameters are presented in Table 2.

Table 1

Doubly fed induction generator parameters

Rated power, P_n	1.5 MW
Rated current, I_n	1900 A
Rated dc-Link voltage U_{DC}	1200
Stator rated voltage, V_s	398/690 V
Stator rated frequency, f	50 Hz
Rotor inductance, L_r	0.0136
Stator inductance, L_s	0.0137
Mutual inductance, M	0.0135
Rotor resistance, R_r	0.021
Stator resistance, R_s	0.012
Number of pair of poles, p	2

Table 2

Wind turbine parameters

Number of blades	3
The power coefficient, $Cpmax$	0.59
Rotor radius, R	35.25 m
Speed multiplier gain, G	90
The density of the air, ρ	1.225 kg/m^3
Moment of total inertia, J	1000 Kg.m^2
Viscous friction coefficient, fr	0.24 s^{-1}

7. SIMULATION RESULTS

To demonstrate the effectiveness of the proposed ANN-DPC strategy, a comparative study between the FOC, C-DPC and the ANN-DPC control.

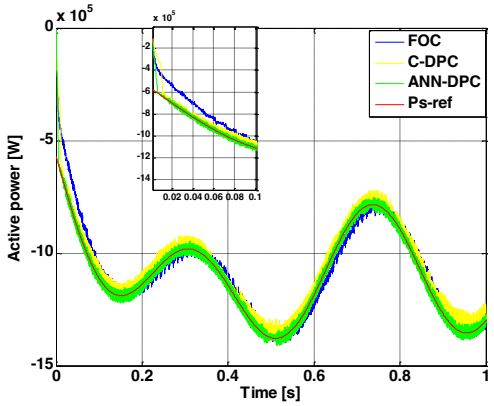

(a)

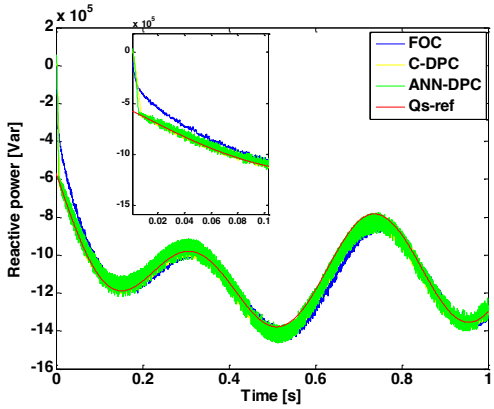

(b)

Fig. 8 – System response ((a): active power (b): reactive power)

The simulation results shown in Fig. 8, clearly show the high performance in the ANN-DPC case following a setpoint change, the ANN-DPC reaches its reference quickly, without exceeding the setpoint with respect to the FOC consequence and C-DPC.

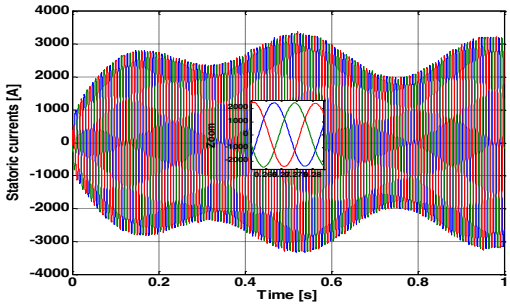

(a)

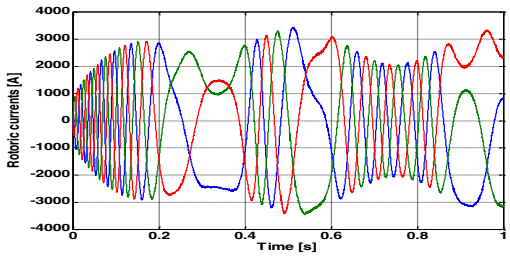

(b)

Fig. 9 – FOC ((a): stator currents, (b): rotor currents)

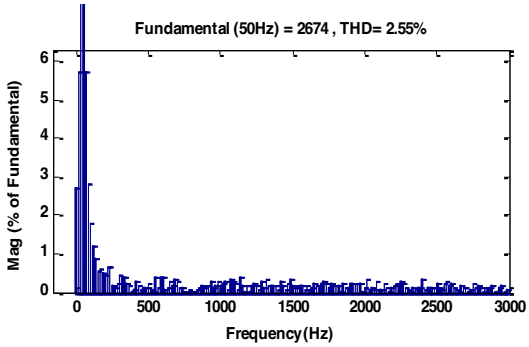

Fig. 10 – Spectrum harmonic of a one-phase stator current (FOC)

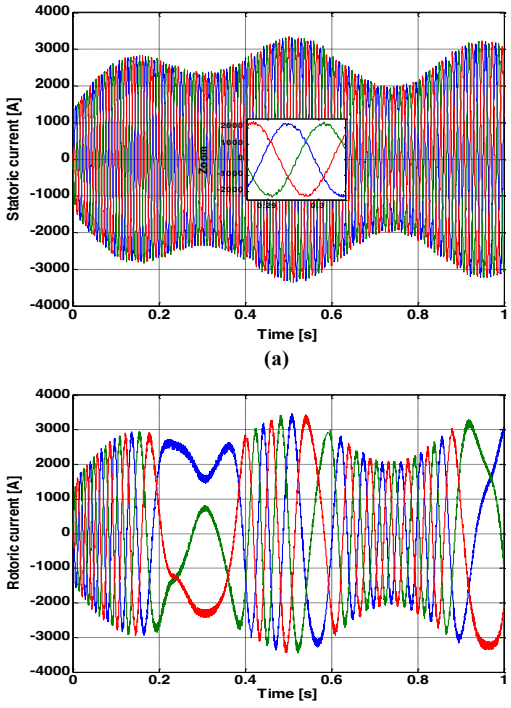

Fig. 11 – C-DPC ((a): Stator currents, (b): Rotor currents)

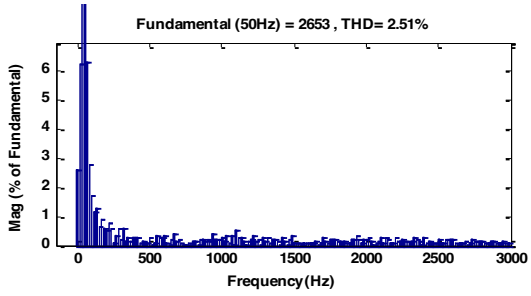

Fig. 12 – Spectrum harmonic of a one-phase stator current (C-DPC)

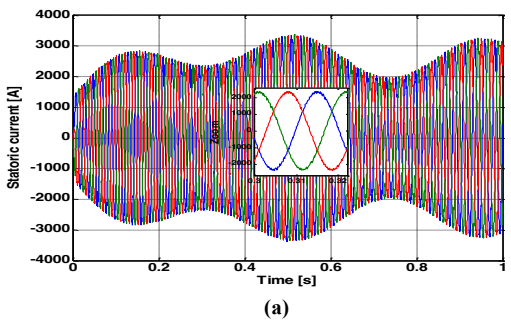

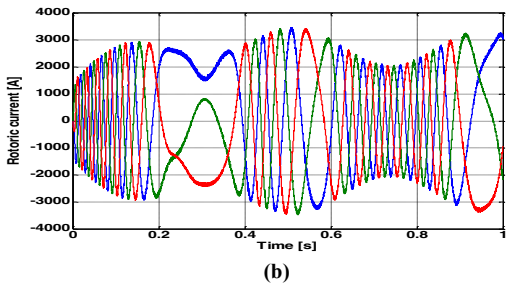

Fig. 13 – ANN-DPC ((a): stator currents, (b): rotor currents)

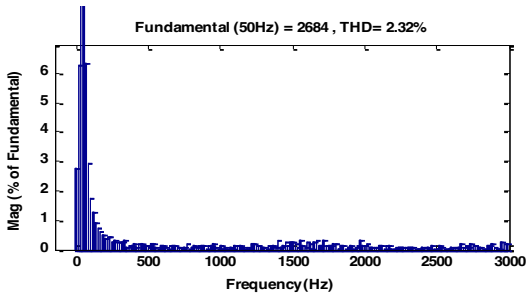

Fig. 14 – Spectrum harmonic of a one-phase stator current (ANN-DPC)

Moreover, the results presented in Figs. 9, 11, and 13 show that the three-phase stator and rotor currents generated by the DFIG are proportional to the active power supplied. The waveform of the currents is almost sinusoidal for the stator current, which means a good quality of energy supplied to the network.

One can also note the passage from hypo-synchronous to hyper-synchronous at times 0.3 s, 0.6 s, and 0.9 s because the stator and rotor powers are equal (Fig. 9-b, Fig. 11-b, Fig. 13-b).

Figure 14 shows the results obtained from the spectral analysis of the currents of the ANN-DPC strategy, namely the stator current. These results show that the ANN-DPC guarantees a better quality of the waveform of the stator current, whose harmonic distortion rate (THD) goes from 2.55 % for the FOC (Fig. 10) and 2.51 % for the C-DPC (Fig. 12) to 2.32 % for the ANN-DPC.

Table 3

Comparison of the performances of the three regulators.

	Regulators		
Performances	FOC	C-DPC	ANN-DPC
Response time *Ps* (*ms*)	90	15	10
Response time *Qs* (*ms*)	95	14	10
Active and reactive power control	Indirectly controlled by rotor currents	Directly controlled	Directly controlled
Computational complexity	High	Low	Low
Transitory response	Medium	Very good	Very good
THD (%)	2.55	2.51	2.32

Table 3 summarizes an overall comparison between FOC, C-DPC, and ANN-DPC regarding the THD. The proposed wind energy system with ANN-DPC achieved the best performance. Nevertheless, due to the fractional-order control strategy proposed in this paper, the current THD with either FOC, C-DPC, or ANN-DPC is lower than 5% limit imposed by IEEE Std 519™-2014 [29].

8. **CONCLUSION**

An ANN-DPC control is proposed to control the active and reactive powers between the DFIG generator and the electricity grid used in a wind turbine system.

The simulation results have shown that applying a neural network gives a good response of active and reactive power. Power level ripples are lower than conventional a FOC and C-DPC techniques, which is reflected in the quality of the currents generated by the DFIG.

From the comparative study between the proposed controller and the conventional C-DPC and FOC controller, it has been shown that the proposed ANN is very effective in the stabilization of the system. Therefore, the proposed method can contribute to expanding wind energy utilization.

Received on 4 June 2020

REFERENCES

1. ***Rapport, *Le baromètre éolien ; systèmes solaires, journal des énergies renouvelables*", *183*, Union Européen (Février 2008).
2. L. Tuan, M.Q. Duong, G.N. Sava, V. Tanasiev, *Optimization of renewable energy sources operation in Vietnam's electricity market*, Rev. Roum. Sci. Techn. – Électrotechn. Et Énerg., **65**, *4*, pp. 221–217, 2020.
3. S. Abdelmalek, L. Barazane, A. Larabi, *Fault diagnosis for a doubly fed induction generato*r, Revue Roumaine des Sciences Techniques–Électrotechnique et Énergetique, **61**, *2*, pp. 159–163 (2016).
4. H. Nian, Y. Song, P. Zhou, Y. He, *Improved direct power control of a wind turbine driven doubly fed induction generator during transient grid voltage unbalance*, IEEE Trans. Energy Convers., **26**, *3*, pp. 976–986, Sep. 2011.
5. S. Arezki, M. Boudour, *Study and regulation of dc bus voltages of wind-photovoltaic system*, Rev. Roum. Sci. Techn. – Électrotechn. et Énerg., **59**, *1*, pp. 35–46 (2014).
6. O. Bachir, A.F. Zoubir, *Comparative analysis of robust controller based on classical proportional-integral controller approach for power control of wind energy system*, Revue Roumaine des Sciences Techniques–Électrotechnique et Énergetique, **63**, *2*, pp. 210–216 (2018).
7. A.M. Eltamaly, M.S. Al-Saud, A.G. Abo-Khalil, *Dynamic control of a DFIG wind power generation system to mitigate unbalanced grid voltage*, IEEE Xplore, IEEE, pp. 39091–39103
8. S. Siniscalchi-Minna, M. De-Prada-Gil, F.D. Bianchi, C. Ocampo-Martinez, B. De Schutter, *A multi-objective predictive control strategy for enhancing primary frequency support with wind farms*, IOP Conf. Series: Journal of Physics: Conf. Series 1037 (2018).
9. I. Yaichi, A. Semmah, M. Djlaila, A. Harrouz, S. Mansouri, Y. Bakou, *'Modelling and control of doubly fed induction machine, application for a wind turbine System*, IEEE Xplore Digital Library, International Renewable and Sustainable Energy Conference (IRSEC), Marrakech, Morocco (2016).
10. O. Aouchenni, R. Babouri, K. Ghedamsi, D. Aouzellag, *Wind farm based on doubly fed induction generator entirely interfaced with power grid through multilevel inverter*, Rev. Roum. Sci. Techn.– Electrotechn. et Energ., **62**, *2*, pp. 170–174 (2017)
11. A. Beddar, H. Bouzekri, B. Babes, H. Afghoul, *Real time implementation of improved fractional-order proportional-integral controller for grid connected wind energy conversion system*, Rev. Roum. Sci. Techn.– Electrotechn. et Energ., **61**, *4*, pp. 402–407 (2016).
12. O. Bachir, A-F, Zoubir, *Comparative analysis of robust controller based on classical proportional-integral controller approach for power control of wind energy system*, Rev. Roum. Sci. Techn.– Electrotechn. et Energ., **63**, *2*, pp. 210–216 (2018).
13. A. Tapia, G. Tapia, *Modeling and control of a wind turbine driven doubly fed induction generator*, IEEE Tran. on Energy Conversion, **18**, *2*, pp. 194–204 (2003).
14. I. Yaichi, A. Semmah, P. Wira, Y. Djeriri, *'Super-twisting sliding mode control of a doubly-fed induction generator based on the SVM strategy*", Periodica Polytechnica Electrical Engineering and Computer Science, **63**, *3*, pp. 178–190 (2019).
15. A. Izanlo, M.V. Kazemi, A. Gholamian, *A new method of predictive direct torque control for doubly fed induction generator under unbalanced grid voltage*, Rev. Roum. Sci. Techn.– Électrotechn. et Énerg., **63**, *3*, pp. 332–337, (2018).
16. Y.K. Wu, W.H. Shu, H.Y. Cheng, G.T. Ye, D.C. Jiang, *Mathematical modelling and simulation of the DFIG-based wind turbine*, CACS International Automatic Control Conference, 2nd ed., **3**, pp. 15–64 (2014).
17. Hu, Y. Huang, D. Wang, H.Y X. Yuan, *Modeling of grid-connected DFIG-based wind turbines for dc-link voltage stability analysis*, IEEE Transactions on Sustainable Energy, **6**, *4*, pp. 1325–1336 (2015).
18. S. Bellarbi, D.S. Koussa, *Fuzzy robust control of double fed induction generator with parameter uncertainties*, Rev. Roum. Sci. Techn.– Électrotechn. et Énerg., **61**, *4*, pp. 367–371 (2016).
19. I. Ngom, A.B. Mbou, L. Thiaw, *Active and reactive power control of doubly fed-induction generator based on variable speed wind power generation*, International Conference on Electrical, Control, Automation and Robotics ECAR 2018.
20. A. Khajeha, Z. Shabani, *Adaptive gain scheduling control of doubly fed induction generator based wind turbines to improve fault ride through performance*, Int. J. of Industrial Electronics, Control and Optimization, **1**, *1*, pp. 61-70 (June 2018).
21. A. Azib, D. Ziane, T. Rekioua, A. Tounzi, Robustness of the direct torque control of double star induction motor in fault condition, Rev. Roum. Sci. Techn.– Électrotechn. et Énerg., **61**, *1*, pp. 147–152 (2016).
22. A. Aberbour, K. Idjdarene, Z. Boudries, Adaptable sliding mode control for wind energy application, Rev. Roum. Sci. Techn. – Électrotechn. et Énerg., **61**, *3*, pp. 258–262 (2016).
23. M.J. Zandzadeh, A. Vahedi, *Modelling and improvement of direct power control of DFIG under unbalanced grid voltage condition*, Int. J. of Electrical Power and Energy Systems, **59**, pp. 58-68 (Jan 2014).
24. P.T. Sharadbhai, S. Gupta, *Artificial neural network based control of doubly fed induction generator for active filtering capabilities*, IEEE Xplore, 2021 4th International Conference on Recent Developments in Control, Automation & Power Engineering (RDCAPE), Noida, India.
25. A. Asri, Y. Mihoub, S. Hassaine, P.O. Logerais, A. Amiar, T. Allaoui, *An adaptive fuzzy proportional integral method for maximum power point tracking control of permanent magnet synchronous generator wind energy conversion system*, Rev. Roum. Sci. Techn. – Électrotechn. Et Énerg., **63**, *3*, pp. 320-325 (2018).
26. Y.A. Ali, M. Ouassaid, *Advanced control strategy of DFIG based wind turbine using combined artificial neural network and PSO algorithm*", IEEE Xplore, 2020 International Conference on Electrical and Information Technologies (ICEIT), Rabat, Morocco.
27. B.F. Florea, O. Grigore, M. Datcu, *Learning online spatial exploration by optimizing artificial neural networks assisted by a pheromone map*, Rev. Roum. Sci. Techn.– Electrotechn. et Energ., **62**, *2*, pp. 209–214 (2017).
28. N.G. Lantewa, N. Magaji, *Control of doubly fed induction generator of variable speed wind turbine system using neural network*, IEEE Xplore, 2018 International Conference and Utility Exhibition on Green Energy for Sustainable Development (ICUE), Phuket, Thailand.
29. ***IEEE Standards Association *IEEE Std 519™-2014 IEEE Recommended Practice and Requirements for Harmonic Control in Electric Power Systems*, The Institute of Electrical and Electronics Engineers, New York, USA, 2014. https://edisciplinas.usp.br/pluginfile.php/1589263/mod_resource/content/1/IEE%20Std%20519-2014.pdf [Accessed: 11 March 2018].